⌘ *Author's Choice*

THE JOURNAL OF BIOLOGICAL CHEMISTRY VOL. 286, NO. 35, pp. 30606–30614, September 2, 2011

Structural and Functional Studies on the N-terminal Domain of the *Shigella* Type III Secretion Protein MxiG[S]

Received for publication, March 25, 2011, and in revised form, May 24, 2011 Published, JBC Papers in Press, July 7, 2011, DOI 10.1074/jbc.M111.243865

Melanie A. McDowell[‡1], Steven Johnson[‡2], Janet E. Deane[‡2,3], Martin Cheung[§], A. Dorothea Roehrich[§], Ariel J. Blocker[§], James M. McDonnell[¶4], and Susan M. Lea[‡5]

From the [‡]Sir William Dunn School of Pathology, University of Oxford, Oxford OX1 3RE, United Kingdom, the [¶]Department of Biochemistry, University of Oxford, Oxford OX1 3QU, United Kingdom, and the [§]Schools of Cellular and Molecular Medicine and Biochemistry, Medical Sciences Building, University of Bristol, University Walk, Bristol BS8 1TD, United Kingdom

MxiG is a single-pass membrane protein that oligomerizes within the inner membrane ring of the *Shigella flexneri* type III secretion system (T3SS). The MxiG N-terminal domain (MxiG-N) is the predominant cytoplasmic structure; however, its role in T3SS assembly and secretion is largely uncharacterized. We have determined the solution structure of MxiG-N residues 6–112 (MxiG-N(6–112)), representing the first published structure of this T3SS domain. The structure shows strong structural homology to forkhead-associated (FHA) domains. Canonically, these cell-signaling modules bind phosphothreonine (Thr(P)) via highly conserved residues. However, the putative phosphate-binding pocket of MxiG-N(6–112) does not align with other FHA domain structures or interact with Thr(P). Furthermore, mutagenesis of potential phosphate-binding residues has no effect on *S. flexneri* T3SS assembly and function. Therefore, MxiG-N has a novel function for an FHA domain. Positioning of MxiG-N(6–112) within the EM density of the *S. flexneri* needle complex gives insight into the ambiguous stoichiometry of the T3SS, supporting models with 24 MxiG subunits in the inner membrane ring.

The type III secretion system (T3SS)[6] is essential for infection by many pathogenic Gram-negative bacteria (1), including enteropathogens such as *Salmonella*, *Escherichia*, *Yersinia*, and *Shigella* spp. The primary focus of this study is *Shigella flexneri*, which invades cells of the intestinal tract and leads to more than 1 million deaths annually from shigellosis (2). The T3SS protein export apparatus functions as a molecular syringe, purportedly inserting a contiguous pore into the host-cell membrane to allow the secretion of virulence factors directly into the host cell (3). The main structure, termed the needle complex (NC), comprises a membrane-embedded basal body and a hollow needle that extends from the bacterial cell surface (4). The component proteins are largely conserved between the NCs of different pathogenic bacteria, so studies of model T3SSs can potentially have widespread therapeutic implications (5, 6). EM has shown that the needle shares a similar morphology with bacterial flagella (7–9). In *S. flexneri*, multiple copies of MxiG, MxiJ, MxiD, and MxiM form the stacked rings of the basal body (10–12), of which the only high resolution structure available is that of MxiM (13, 14). The *Salmonella* sequence homologues of MxiG and MxiJ (PrgH and PrgK, respectively) have been shown to account for the electron density of the inner membrane rings (IMR) (15, 16), whereas the MxiD homologue, InvG, is localized to the outer membrane and reaches deep down into the periplasm (16). Two concentric rings form the IMR of *Salmonella typhimurium* (16). The increased solvent accessibility of PrgH relative to PrgK suggests the PrgH ring is larger and encloses the PrgK ring (17). The stoichiometry of the IMR is still a controversial topic within the field, with current models favoring 12- or 24-subunit rings (16–19). Although atomic structures of the periplasmic domains of MxiG, MxiJ, and MxiD functional homologues (PrgH (18), EscJ (17, 20), and EscC (18), respectively) are available, the relatively low resolution of available EM density maps and a lack of understanding of intermolecular interactions makes placing them within the context of the intact T3SS ambiguous.

Based on secondary structure prediction analysis, MxiG is expected to have a transmembrane domain (residues 127–141) separating two soluble domains (21). Alkaline phosphatase fusions (21) and cryo-EM visualization of Ni^{2+}-NTA nanogold labels (16) concur that the N-terminal domain (MxiG-N; residues 1–126) is localized to the cytoplasmic side of the membrane in assembled needle complexes, whereas the C-terminal domain (MxiG-C; residues 142–371) is in the periplasm. Density attributed to the nanogold labels was more diffuse when MxiG-N was labeled relative to MxiG-C, suggesting a greater flexibility of this domain (16). Indeed, the 70 × 50 Å globular masses at the base of needle complexes that can probably be attributed to MxiG-N (22) show positional variability (19, 23). Specifically, they are observed to undergo a clamping movement when EM images of *Salmonella* basal bodies and intact

[S] The on-line version of this article (available at http://www.jbc.org) contains supplemental Figs. 1–5.

⌘ *Author's Choice*—Final version full access.

The atomic coordinates and structure factors (code 2xxs) have been deposited in the Protein Data Bank, Research Collaboratory for Structural Bioinformatics, Rutgers University, New Brunswick, NJ (http://www.rcsb.org/).

[1] Supported by Wellcome Trust-funded studentship 086833.

[2] Supported by Wellcome Trust Programme Grant 059011 (to S. M. L.).

[3] Present address: Cambridge Institute for Medical Research, Wellcome Trust/MRC Bldg., Addenbrooke's Hospital, Hills Road, Cambridge CB2 0XY, United Kingdom.

[4] Present address: The Randall Division of Cell and Molecular Biophysics, King's College London, Guy's Campus, London SE1 1UL, United Kingdom.

[5] To whom correspondence should be addressed: Sir William Dunn School of Pathology, University of Oxford, Oxford OX1 3RE, United Kingdom. Tel.: 44-1865-275181; Fax: 44-1865-275515; E-mail: susan.lea@path.ox.ac.uk.

[6] The abbreviations used are: T3SS, type III secretion system; NC, needle complex; IMR, inner membrane ring(s); MxiG-N, MxiG N-terminal domain; MxiG-C, MxiG C-terminal domain; CR, Congo red; r.m.s., root mean square; PDB, Protein Data Bank; FHA, forkhead-associated.

needle complexes are compared (23). This suggests MxiG-N is conformationally flexible, which suggests that it may play a role in the substrate specificity of the secretion apparatus. The cytoplasmic portion of MxiJ is only 10 residues (24), so MxiG-N is the predominant basal body structure in the cytoplasm, indicating a possible role in communicating cytoplasmic signals to the rest of the T3SS.

In addition to a role in cell signaling, MxiG-N could also function in the structural stabilization of the IMR via self-association. Some EM reconstructions show a continuous ring of density in the region thought to correspond to MxiG-N at the base of the NC (19, 23), whereas others indicate a discontinuous ring (22). Therefore, it is currently unclear whether MxiG-N domains are in close enough proximity to oligomerize.

Although MxiG has few close sequence homologues, many T3SS have putative functional counterparts localized to the inner membrane and with a similar domain organization. The single-pass inner membrane protein YscD from *Yersinia* spp. is required for secretion by the T3SS (25), and the C-terminal domain shows long stretches with up to 28% identity to MxiG-C, indicating that YscD is the likely structural homologue of MxiG. Recently, the YscD domain equivalent to MxiG-N has been shown to be essential for protein secretion by the *Yersinia pestis* T3SS (26). Roles for MxiG-N in signaling or structural stabilization within the T3SS can be postulated, but the function of this prominent basal body component is largely uncharacterized. Because the MxiG-N sequence gives no clue about the domain function, we must rely on structural homology to gain an insight. There are currently no published high resolution structures available for any domain homologous to MxiG-N, identifying it as an important structural target.

EXPERIMENTAL PROCEDURES

Gene Cloning, Expression, and Purification of MxiG-N(6–112) for Structure Determination—The *mxiG* coding region corresponding to residues 1–126 was amplified using polymerase chain reaction (PCR) (forward, 5′-CGCGGCAGCCATATGTCTG-AGGCAAAGAACTCAAATCTT-3′; reverse, 5′-TTAGC-AGCCGGATCCTTACGAGTGGTTCTTATACATTCC-3′). The PCR product was subcloned into the NdeI and BamHI sites of a pET14b vector (Merck) using the In-Fusion™ PCR cloning system (Clontech). The pET14b-MxiG-N(1–126) plasmid was transformed into *Escherichia coli* BL21 (DE3) pLysS for overexpression. Cells were initially grown to the exponential phase in LB medium before transfer to $^{13}C/^{15}N$-labeled M9 minimal medium containing 100 μg/ml ampicillin. Growth was at 37 °C until $A_{600\,nm}$ of ~0.5 was reached, and then protein expression was induced overnight at 20 °C with 0.4 mM IPTG. Cells were harvested by centrifugation (30 min, 4000 × *g*, 4 °C), resuspended in lysis buffer (50 mM Tris (pH 7.5), 500 mM NaCl, 1 mM DTT, and Complete EDTA-free protease inhibitor mixture (Roche Applied Science)) and lysed at 15,000 p.s.i. using an Emulsiflex-C5 Homogenizer (GC Technologies). The homogenate was centrifuged (30 min, 26,000 × *g*, 4 °C) and loaded onto a 5-ml Ni^{2+}-NTA superflow cartridge (Qiagen). The column was washed with 50 mM imidazole, and protein was eluted with 300 mM imidazole. Eluted fractions were dialyzed overnight in a 3500 molecular weight cut-off snakeskin tubing (Pierce) against 4 × 1l dialysis buffer (50 mM Tris (pH 7.5), 150 mM NaCl). Limited proteolysis was carried out on MxiG-N(1–126) at a protein/trypsin ratio of 250 μg to 1 μg for 2 h at room temperature, producing MxiG-N(6–112). The protein was further purified using a HiLoad 26/60 Superdex 75 pg (GE Healthcare) column preequilibrated in 25 mM Na_2HPO_4 (pH 6.8), 1 mM DTT. The eluted fractions were concentrated to 0.5 ml (2–5 mM) using Vivaspin 20 5kDa molecular mass cut-off centrifugal devices (GE Healthcare).

Expression and Purification of MxiG-N(6–112) for NMR Titrations—MxiG-N(1–126) was overexpressed in ^{15}N-labeled M9 minimal medium and purified as for the doubly labeled protein. Size exclusion chromatography of MxiG-N(6–112) was with 100 mM Tris (pH 7.5), 50 mM NaCl, 1 mM DTT. The eluted fractions were concentrated to 250 μM.

NMR Spectroscopy and Structure Determination—5% (v/v) D_2O was added to all samples. All spectra were recorded at 25 °C on Bruker 500- and 700-MHz spectrometers. ^1H, ^{13}C, and ^{15}N assignments of MxiG-N(6–112) were achieved using a suite of triple resonance multidimensional experiments (HN(CO)CA (27), CBCA(CO)NH (28), CBCANH (29), HNCO (30), CC(CO)NH (31), H(CCCO)NH) and analysis with Sparky (32). Interproton distance restraints were obtained from three-dimensional ^{15}N NOESY-HSQC (33) and ^{13}C NOESY (>98% D_2O) experiments. Peak volumes were calibrated to distances assuming a typical $d_{\alpha\alpha}$ distance of 2.3 Å across antiparallel β-strands for the ^{13}C NOESY spectrum and a typical sequential $d_{\alpha N}$ distance of 2.2 Å within antiparallel β-strands for the ^{15}N NOESY-HSQC spectrum (34). Slowly exchanging amide protons were shown by a series of $^1H,^{15}N$ HSQC spectra collected over 20 h after buffer exchange of the sample with D_2O buffered by 25 mM Na_2HPO_4, 1 mM DTT. These data were used in conjunction with a long range H(N)CO experiment (35) to identify hydrogen bonds, providing distance restraints of 2.0–2.5 Å (H–O) and 3.0–3.5 Å (N–O). Restraints for the backbone torsion angles Φ and Ψ were derived from TALOS+ (36). Structure calculations using the experimentally derived distance and torsion angle restraints were carried out using DYANA-1.5 (37), which performs simulated annealing by molecular dynamics in torsion angle space. From 350 calculated structures, the 20 with the lowest target function were selected.

An NMR titration with phosphothreonine (Thr(P)) (Bachem) was carried out by collecting a $^1H,^{15}N$ HSQC spectrum after the addition of 50 mM Thr(P) buffered in 100 mM Tris (pH 7.5), 50 mM NaCl.

Site-directed Mutagenesis—The QuikChange XL site-directed mutagenesis kit (Stratagene) was used to introduce S61A/S63A mutations (Table 1) into the pAB13 construct (21), as verified by sequencing of plasmid DNA from Miniprep spin purification (Qiagen) with the M13F and M13R primers. An R39A mutation was subsequently introduced into the S61A/S63A-pAB13 construct to create a triple R39A/S61A/S63A mutant.

Overnight Leakage and Congo Red Induction Assays—*S. flexneri* strains (Table 2) were transformed with 100 ng/μl plasmid by electroporation and phenotypically selected on Congo red (CR) agar plates (38). Strains were grown in tryptic casein soy broth with the indicated antibiotics at the following final con-

TABLE 1
Primers for site-directed mutagenesis

Mutation	Forward primer	Reverse primer
R39A	5′-CTTAATTGTTCTCGGAGCGACGATAGAAACACTTGAG-3′	5′-CTCAAGTGTTTCTATCGTCGCTCCGAGAACAATTAAG-3′
S61A/S63A	5′-CCTGTAACAGATGCTAAAGCGGATGGTATAATTTATTTG ACCATAAG-3′	5′-CTTATGGTCAAATAAATTATACCATCCGCTTTAGCATC TGTTACAGG-3′

TABLE 2
***S. flexneri* strains**

Strain	Genotype (strain, plasmid)	Resistance	Reference/Source
WT	Wild-type M90T, serotype 5a		Ref. 70
mxiG^{-}	SF703	Kan^{R}	Ref. 21
mxiG$^{-/+}$	SF703 + pAB13	Kan^{R}, Amp^{R}	Ref. 21
mxiG$^{-/mutant}$	SF703 + pAB13-R39A/S61A/S63A	Kan^{R}, Amp^{R}	This study
WT/pBAD-MxiGN	Wild-type M90T, serotype 5a + pBAD-MxiGN	Amp^{R}	This study

centrations: kanamycin, 50 μg/ml; ampicillin, 100 μg/ml. Overnight leakage and CR induction assays were performed as described previously (39). 20 μl of bacterial supernatant was separated by SDS-PAGE and silver-stained with the SilverXpress kit (Invitrogen).

The pBAD-MxiGN construct was made by PCR amplification of residues 2–125 from the *mxiG* coding sequence (forward, 5′-AGCCATAGATCTGAGGCAAAGAACTCAAATCTTGCACC-3′; reverse, 5′-GCATCAGGTACCCTAGTGGTTCTTATACATTCCGTTTAGTATATGGCC-3′) and subcloning of the resulting fragment into the BglII and KpnI sites of pSZ1 (40). Overexpression of MxiG-N(2–125) in the WT/pBAD-MxiGN strain (Table 2) was induced with 0.02 or 0.2% arabinose. Whole cell lysates were separated by SDS-PAGE, and Western blotting was performed with a mouse monoclonal anti-MxiG antibody (40).

Multiangle Light Scattering with MxiG-N(6–112)—Unlabeled MxiG-N(1–126) was produced by expressing pET14b-MxiG-N(1–126) in B834 (DE3) pLysS in LB for 3 h at 37 °C and then following the same purification protocol as for the doubly labeled protein, except the dialysis and limited proteolysis steps were omitted. The running buffer for size exclusion chromatography was 50 mM Tris-HCl (pH 7.5), 150 mM NaCl, 1 mM DTT. MxiG-N(1–126) was concentrated to 0.45 mM for multiangle light scattering. Multiangle light scattering was carried out with a multiangle light photometer (Dawn Heleos II, Wyatt) connected to a high pressure liquid chromatography (HPLC) system (Agilent Technologies 1200 series) to which a Superdex 200 10/300 GL size exclusion column was attached.

Fitting of the Model in the EM Reconstruction—The coordinates of the lowest energy MxiG-N(1–126) model were manually fitted into the leg density of the C24 *S. flexneri* EM map (EMDB 6391) (19) using Coot (41). 24 copies of the model were generated by sequential rotations of 15° around the rotational axis of the map. Correlation coefficients were calculated using MAPMAN (42) between the leg density ring (cut out of the needle complex map using CCP4-MAPROT) and the model map (created using CCP4-SFALL and CCP4-FFT) (43). A model for full-length MxiG was created using MxiG-N(1–126), a 20-residue helix, and a SCWRL (44, 45) model based on the periplasmic domain of PrgH (Protein Data Bank (PDB) entry 3GR0).

RESULTS

Solution Structure of MxiG-N(6–112)—A 16.5-kDa construct for the MxiG-N domain containing residues 1–126 and a 20-residue MGSSHHHHHHSSGLVPRGSH N-terminal tag (MxiG-N(1–126)) gave rise to a ^{1}H,^{15}N HSQC spectrum that was unassignable due to peak overlap. Mass spectrometry analysis showed that limited proteolysis with trypsin removed the tag and termini, forming a 12.2-kDa construct containing residues 6–112 (MxiG-N(6–112)). The ^{1}H,^{15}N HSQC shows good peak dispersion in both dimensions and agrees well with peak positions from the MxiG-N(1–126) spectrum, indicating that the improvement in spectral quality is due to removal of the flexible termini (supplemental Fig. 1). All 102 non-proline backbone amides and 15 asparagine/glutamine side chain amides were assigned via a suite of three-dimensional triple resonance NMR experiments (Fig. 1). This facilitated the subsequent assignment of side-chain atoms and the determination of input restraints for the structure calculation.

A family of 350 structures for MxiG-N(6–112) was calculated using the program DYANA (37), and the 20 structures with the lowest target function were taken for the final ensemble (Fig. 2, *A* and *B*). The structural statistics (Table 3) indicate that the structures minimally violate the input restraints, are well defined, and have a good covalent geometry.

The final family of structures (Fig. 2, *A* and *B*) are highly convergent and precisely define the three-dimensional solution structure of MxiG-N(6–112), with a backbone root mean square (r.m.s.) deviation of 0.52 ± 0.07 Å (Table 3). The topology is one α-helix and nine β-strands, arranged as a four-stranded antiparallel β-sheet and a five-stranded β-sheet with three antiparallel strands and a β-α-β motif (Fig. 2*C*). These two β-sheets pack against each other to form a globular structure. The calculated structures diverge at the N and C termini, between residues Glu-45 and Phe-51 (loop 1) and between residues Ile-89 and Gln-92 (loop 2). These regions correlate with low heteronuclear ^{1}H,^{15}N NOE values, suggesting that they are poorly constrained as a result of true backbone flexibility. The electrostatic surface of MxiG-N(6–112) calculated using APBS (46) shows one face of the molecule to have a large positively charged patch (Fig. 2*D*), whereas the opposing face is predominantly negatively charged (Fig. 2*E*).

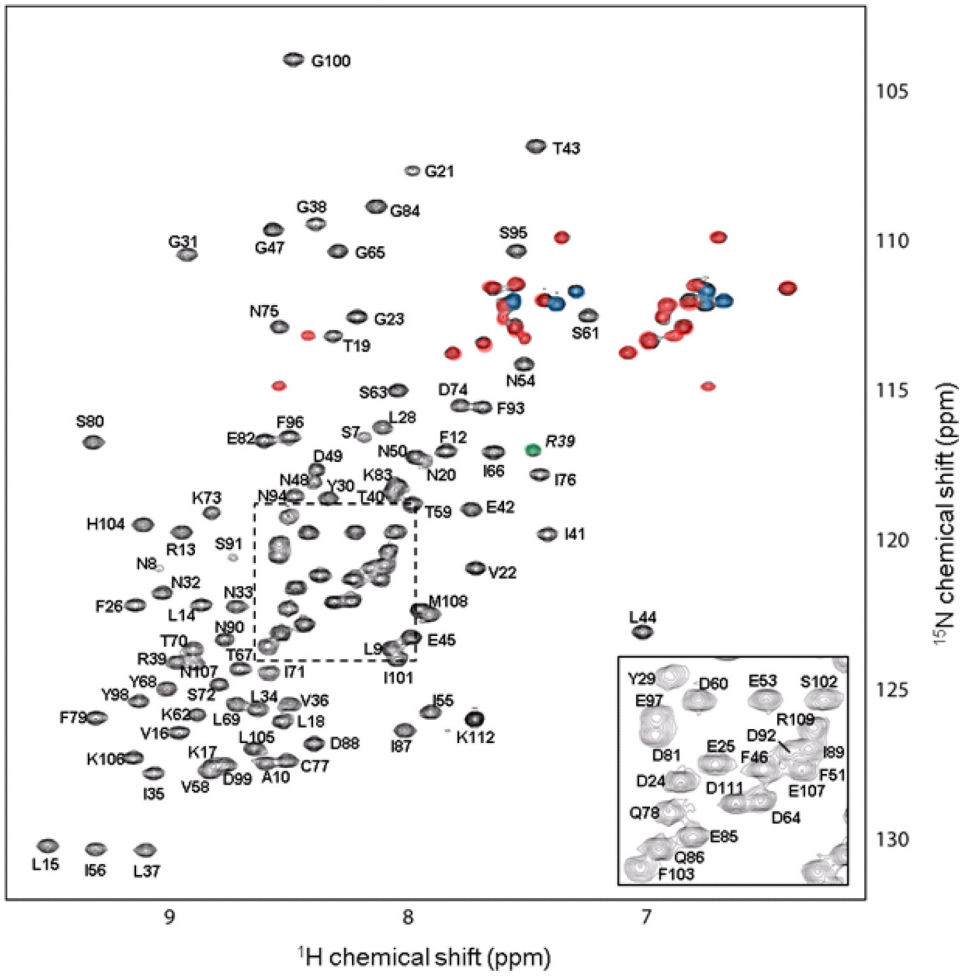

FIGURE 1. **^{1}H,^{15}N HSQC spectrum of MxiG-N(6–112).** Assignments of backbone amides are shown. Peaks corresponding to backbone amides, asparagine side chains, glutamine side chains, and arginine side chains have been artificially *color-coded* as *black*, *red*, *blue*, and *green*, respectively. Assignment of the side-chain amide of Arg-39 (*R39*) is shown in *italic type*. The *zoomed inset* corresponds to the region of the spectrum indicated by the *dashed box*.

MxiG-N(6–112) Has the Fold of a Forkhead-associated Domain—A structural homology search of the PDB with the coordinates of the top model of MxiG-N(6–112) using the DALI algorithm (47), identified structures of forkhead-associated (FHA) domains, with the best 50 matches having a DALI *Z*-score of 8.3–5.9. The closest structural homologue is the FHA domain of CT664 from *Chlamydia trachomatis* (DALI *Z*-score 8.3, PBD entry 3gqs), which shows a striking similarity of protein fold and particularly good alignment of β-strands when superimposed on MxiG-N(6–112) (Fig. 2*F*).

FHA domains act as phosphothreonine (Thr(P)) binding modules in cell signaling, regulating a diverse range of functions in both prokaryotic and eukaryotic proteins (48). The FHA fold is composed of ~75 amino acids and contains three highly conserved motifs: a GR dipeptide at the end of strand 3, an S*XX*H sequence before strand 5, and an NG motif before strand 7. These motifs have been shown to be crucial for phosphothreonine binding and binding site stabilization (49, 50). The MxiG-N(6–112) sequence only has four of these six conserved residues present in the expected positions relative to secondary structure: Gly-38, Arg-39, Ser-61/63, and Gly-84. To ascertain the structural alignment of Arg-39 and Ser-61/63 with their highly conserved counterparts, the MxiG-N(6–112) model with the lowest target function was superimposed on functional FHA domains from *Saccharomyces cerevisiae* Rad53 (DALI *Z*-score 6.0, PDB Bank entry 2jqi) (51), *Mycobacterium tuberculosis* EmbR (DALI *Z*-score 7.1, PDB entry 2fez) (52), and human Ki67 (DALI *Z*-score 7.1, PDB entry 2aff) (53). The r.m.s. deviation values for the loop regions of interest suggest that these are well ordered portions of the MxiG-N(6–112) ensemble, so the top model is likely to be representative of the native conformation. Although Arg-39 and Ser-61/63 are in the expected loop regions, alignment of their side chains with those of the conserved residues is poor, particularly for Ser-61 and Ser-63. (Fig. 3). Therefore, it would seem unlikely that they could assume their traditional role in direct coordination of phosphate (50, 54). Gly-84 is not found within the context of an NG motif and is structurally distant from the equivalent glycine residues of other FHA domains, suggesting that Gly-84 may not be a structurally equivalent residue. In addition, MxiG-N(6–112) lacks the conserved histidine and asparagine residues required to stabilize the binding site architecture (54). It is therefore unlikely that MxiG-N has the residue arrangement required to form a functional phosphate-binding pocket.

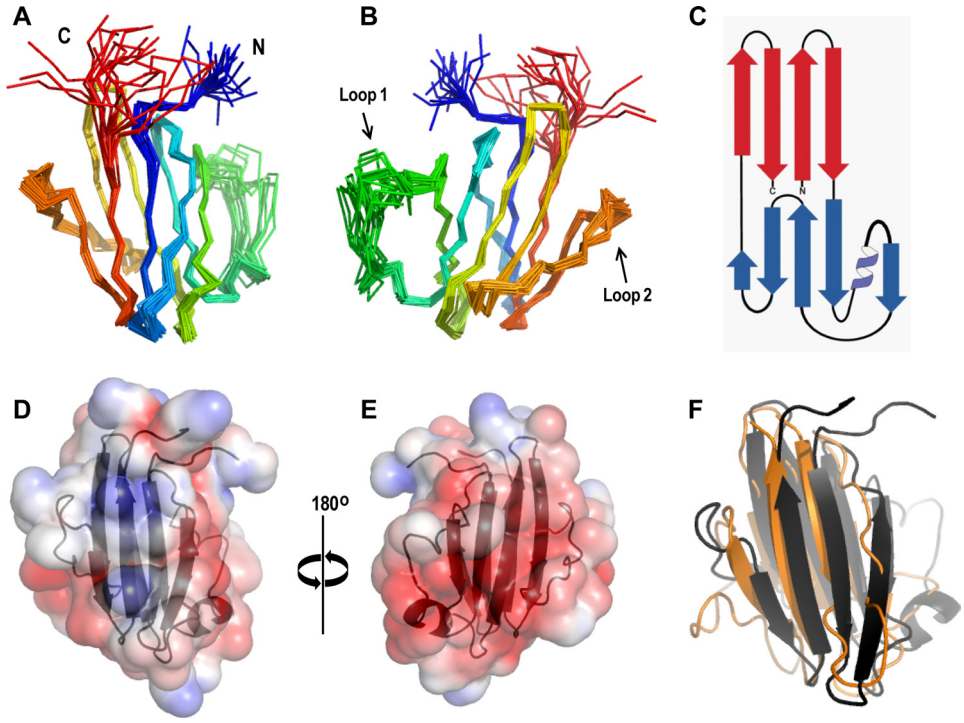

FIGURE 2. **The NMR structure of MxiG-N(6–112).** *A* and *B*, backbone superimposition of the final 20 structures by residues 13–38, 54–81, and 93–106. Structures are *colored* from the N terminus (*blue*) to the C terminus (*red*). Termini and flexible loops are indicated. *C*, topology of MxiG-N showing β-sheet 1 (*red*) and β-sheet 2 (*blue*). *D* and *E*, electrostatic surface of MxiG-N(6–112) showing positive (*blue*) and negative (*red*) regions. *F*, overlay of *ribbon diagrams* of MxiG-N(6–112) (*black*) and CT664 (*orange*; PBD entry 3gqs). MxiG-N(6–112) is represented by the structure with the lowest target function.

TABLE 3
Summary of restraints and structural statistics for MxiG-N(6–112)

Parameter	Value
Construct information	
Residues	107
Atoms	1694
No. of restraints	
NOEs used in structure calculation	
Sequential	355
Medium range (2–4 residues apart)	75
Long range (≥5 residues apart)	408
Total interresidue NOEs	838
Dihedral angles from TALOS+ (Φ and Ψ)	183
Hydrogen bonds	37
Total no. of restraints	1058
Violations	
No. of violations:	
Distance restraints (≥0.5 Å)	0
Dihedral angle restraints (≥5°)	0
Violations (average over 20 structures):	
Distance restraints (Å)	0.010 ± 0.001
Dihedral angle restraints (degrees)	0.003 ± 0.001
Target function (Å^2)	2.06 ± 0.16
Precision[a]	
Backbone heavy atoms (Å)	0.52 ± 0.07
All heavy atoms (Å)	1.28 ± 0.11
Structure quality[b]	
Residues in favoured regions	94.0%
Residues in allowed regions	99.9%

[a] Values reported as the average over 20 structures. r.m.s. deviation was calculated by pairwise superimposition of the structures. The structure is defined as residues 13–38, 54–81, and 93–106.
[b] Determined using MolProbity (69) for residues 11–107 of 20 structures.

MxiG-N(6–112) Does Not Have the Canonical Function of a FHA Domain—To investigate whether MxiG-N(6–112) possesses a functional phosphate-binding site, a 138 μM sample of ^{15}N-labeled protein was titrated with 50 mM Thr(P). The

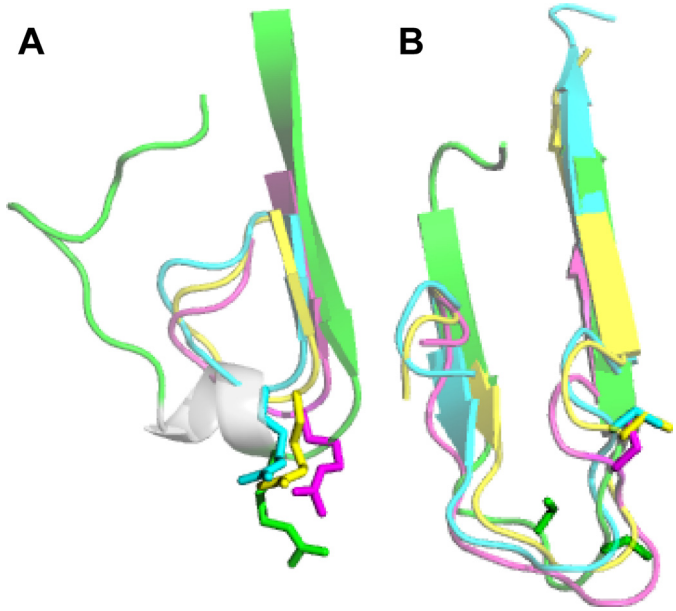

FIGURE 3. **Overlay of *ribbon diagrams* of MxiG-N(6–112) (*green*), Rad53-FHA1 (*magenta*; PDB entry 2jgi), EmbR (*yellow*; PDB entry 2fez), and Ki67 (*cyan*; PDB entry 2aff).** *A*, structural comparison of loop regions containing the conserved arginines. Residues 31–53, 66–75, 309–318, and 28–37 and the side chains of Arg-39, Arg-70, Arg-312, and Arg-31 are shown for MxiG-N(6–112), Rad53-FHA1, EmbR, and Ki67, respectively. Residues 40–43 of MxiG-N(6–112) are *colored gray* for clarity. The heavy atom r.m.s. deviation for residues 37–40 of the MxiG-N(6–112) ensemble is 1.29 ± 0.40 Å. *B*, structural comparison of loop regions containing the conserved serines. Residues 51–71, 73–91, 314–335, and 32–56 and the side chains of Ser-61 and Ser-63, Ser-85, Ser-326, and Ser-45 are shown for MxiG-N(6–112), Rad53-FHA1, EmbR, and Ki67, respectively. The heavy atom r.m.s. deviation for residues 59–63 of the MxiG-N(6–112) ensemble is 1.08 ± 0.34 Å.

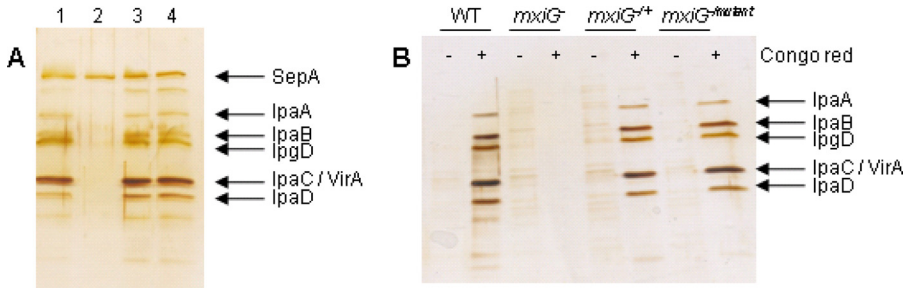

FIGURE 4. **Effect of mutations in the canonical FHA binding site on T3SS assembly and secretion in *S. flexneri* and cellular localization of MxiG-N(1–126).** *A*, samples from the overnight leakage assay run on a 10% SDS-polyacrylamide gel and silver-stained. *Lane 1*, WT; *lane 2*, $mxiG^{-}$; *lane 3*, $mxiG^{-/+}$; *lane 4*, $mxiG^{-/mutant}$. *B*, samples from the Congo red induction assay run on a 10% SDS-polyacrylamide gel and silver-stained. *S. flexneri* strains were exposed to either no CR (−) or 200 μg/ml CR (+).

$^{1}H,^{15}N$ HSQC peak positions show no change as a result of the titration (supplemental Fig. 2), indicating no interaction between MxiG-N(6–112) and a high concentration of Thr(P). Therefore, MxiG-N is unlikely to be involved in cell signaling via phospho-recognition.

Conserved binding residues are required for the functionality of FHA domain-containing proteins (55) and would be expected to play a role in the T3SS if MxiG-N has a canonical FHA Thr(P) recognition site. A R39A/S61A/S63A triple mutation was introduced into full-length MxiG within the pUC19 vector (pAB13 construct) (21), which was subsequently transformed into a $mxiG^{-}$ strain of *S. flexneri 5a* to form $mxiG^{-/mutant}$ (Table 2). The $mxiG^{-/mutant}$ strain gave red colonies on a CR agar plate, providing a preliminary indication of correct T3SS assembly (38, 56). Subsequently, $mxiG^{-/mutant}$ displayed wild-type secretion of early effectors in both overnight leakage (56) and CR induction assays (57) (Fig. 4), suggesting that the mutations have not hindered the assembly of a fully secreting T3SS. Therefore, phospho-recognition by MxiG-N at the conserved interaction site does not regulate any major step in T3SS assembly or function, implying that MxiG-N does not function as a canonical FHA domain.

If MxiG-N has a regulatory role in the T3SS, it would presumably compete for any cytoplasmic *in vivo* interaction partners of MxiG and hinder downstream regulatory pathways when overexpressed in *S. flexneri*. Residues 2–125 of MxiG (MxiG-N(2–125)) were cloned into a derivative of the pSZ1 construct (40). This pBAD-MxiGN construct was subsequently introduced into the WT *S. flexneri* strain to form WT/pBAD-MxiGN (Table 2), and MxiG-N(2–125) was detectably overexpressed with 0.2% arabinose (supplemental Fig. 3*A*). The secretion profile of WT/pBAD-MxiGN indicates a wild-type phenotype (supplemental Fig. 3*B*), suggesting that MxiG-N either does not have a regulatory role in T3SS assembly or function or needs to be localized to the basal body for such a role.

MxiG-N(6–112) Does Not Undergo High Affinity Self-association—MxiG-N may have an alternative structural role in stabilizing the IMR. The oppositely charged faces of MxiG-N(6–112) (Fig. 2, *D* and *E*) indicate that the domain could self-associate via electrostatic interactions. However, no changes in chemical shift positions or peak widths are observed in the $^{1}H,^{15}N$ HSQC of MxiG-N(6–112) over a concentration range of 138 μM to 5 mM. Further, multiangle light scattering suggested that MxiG-N(1–126) does not oligomerize when present at concentrations up to 0.45 mM (supplemental Fig. 4). These data indicate that high affinity interactions between MxiG-N domains are not responsible for structural stabilization of the IMR.

Positioning of MxiG-N(6–112) within the T3SS Is Consistent with 24 MxiG Subunits—The solution structure of MxiG-N(6–112) was manually positioned within the leg domains of the C24 *S. flexneri* EM map (EMDB 6391) (19). The exact orientation was ambiguous due to the low resolution of the map (25 Å) and the lack of asymmetry in the domain; therefore, the position was defined by restraining the C terminus with respect to the likely density for the transmembrane region. Positioning within a side view of the density shows that the size and shape of MxiG-N(6–112) are consistent with the envelope (Fig. 5*A*), supporting the evidence that this region corresponds to MxiG-N (16). When expanded to 24 copies using the symmetry operators of the map (Fig. 5*B*), this model for the cytoplasmic ring agrees well with the experimental map, having a correlation coefficient of 78% and only minor structural clashes between subunits. Our structure is therefore consistent with a model of 24 copies of MxiG forming the outer portion of the inner membrane ring (Fig. 5*C*).

DISCUSSION

The solution structure for MxiG-N(6–112) has been determined, providing the first atomic resolution model of this T3SS domain from a clinically important enteropathogen. The structure shows that MxiG-N has the fold of an FHA domain. This protein fold was originally identified as a phosphothreonine binding module in eukaryotes, for which there is now a good understanding of binding characteristics and their diverse involvement in cell signaling at the structural level (50, 58). A PSI-BLAST search using the Fha1 domain of the DNA damage checkpoint kinase Rad53 from *S. cerevisiae* uncovered putative bacterial FHA domains implicated in many bacterial processes (49); however, their role in bacterial signaling still remains largely uncharacterized. Of particular interest for this study, the N-terminal domain of YscD from *Yersinia enterocolitica* was classified as an FHA domain (49). Chlamydial species also have an FHA domain-containing protein within their T3SS gene cluster (49), which appears to be homologous to YscD (59). Indeed, CT664 from *C. trachomatis* was found to be the closest structural homologue of MxiG-N(6–112). Therefore, a cyto-

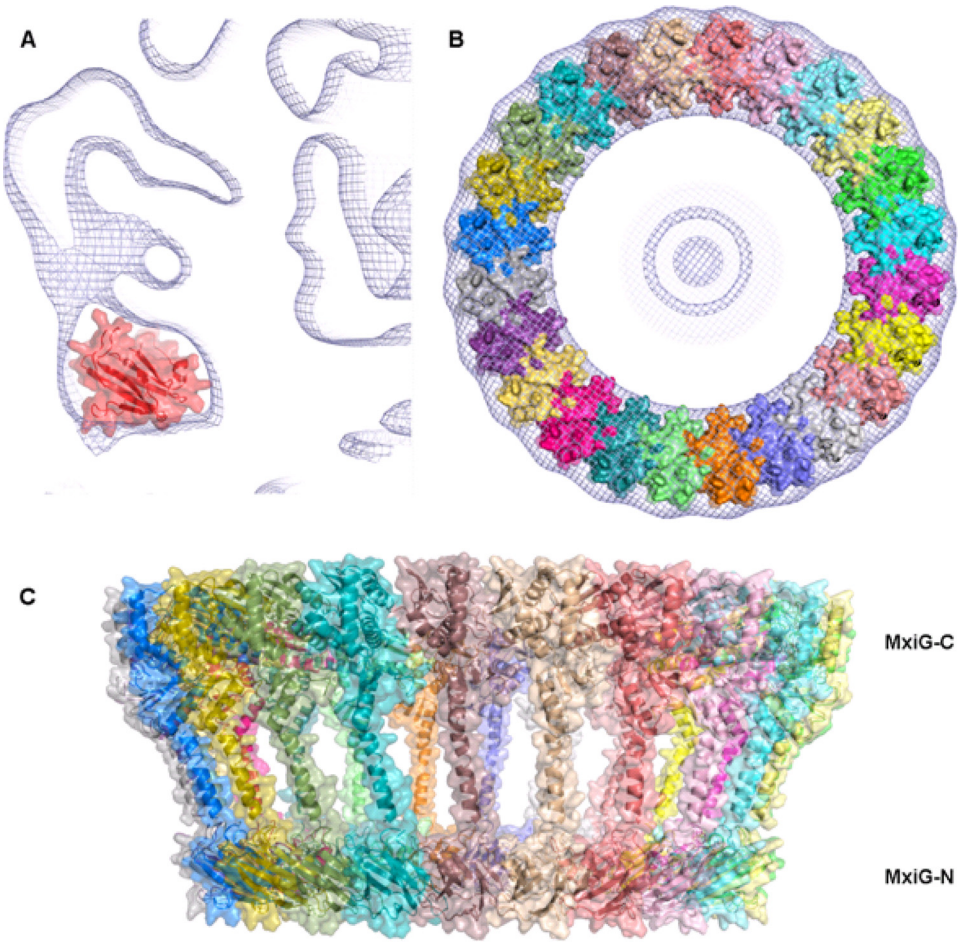

FIGURE 5. **Positioning of MxiG-N(6–112) in the C24 *S. flexneri* NC EM map contoured to 1σ (EMDB 6391).** *A*, a position of MxiG-N(6–112) (*red*) in the density for the leg domains (19), restraining the C terminus with respect to the likely density for the transmembrane region. Due to the globular nature of MxiG-N(6–112) and the low resolution of the density, multiple variations of this positioning cannot be distinguished. However, the volume occupied by a single subunit supports the idea that 24 copies can assemble in the ring. *B*, view of the position of MxiG-N(6–112) as described in *A* symmetrized to give 24 evenly arranged copies within the likely density for the MxiG-N ring. The needle complex base is viewed from the cytoplasmic side. *C*, model for a 24-subunit MxiG ring. MxiG-N is represented by MxiG-N(6–112), whereas MxiG-C is a SCWRL model (44, 45) based on the crystal structure of PrgH(170–362) (PDB entry 3GR0). The transmembrane region is depicted as an arbitrary 20-amino acid helix. Whereas the model shows the likely volume occupied by a 24-member ring, the positioning of the MxiG subunits with respect to each other represents one of many possible conformations given the current data.

plasmic FHA fold appears to be a conserved feature of the MxiG family of proteins, despite a lack of sequence homology.

Given the intimate involvement of an FHA domain in the regulation of the *Pseudomonas aeruginosa* type VI secretion system (60), we questioned whether the T3SS has conserved a FHA fold for a similar canonical role in phosphorylation-mediated cell signaling. Widespread sequence comparison of FHA domains has identified three highly conserved motifs, required for direct substrate binding and binding site stabilization (54). It follows that the presence of these residues could be used to predict whether an FHA domain possesses a canonical binding pocket for Thr(P) peptides. Because MxiG-N lacks the full repertoire of conserved residues, it would not be expected to have a phosphate-binding pocket. We confirmed this by comparing the MxiG-N(6–112) solution structure with other FHA domains, which showed significant structural deviation in the substrate-binding loops. A subsequent NMR titration indicates no interaction between MxiG-N(6–112) and Thr(P), and mutagenesis of conserved binding residues has no affect on the *in vivo* function of the T3SS. Therefore, MxiG-N does not appear to function in cell signaling via phospho-recognition, as would be expected for a canonical FHA domain.

Is this trait shared by the FHA domains of MxiG homologues? The two FHA domains within the cytoplasmic N-terminal region of Cpn0172 from *Chlamydophila pneumonia* were found to interact with and be phosphorylated by the dual specificity kinase PknD (61). Although the physiological significance, if any, of this observation is unknown, it has been speculated from this that the chlamydial T3SS is regulated by reversible phosphorylation. However, FHA-2 of Cpn0172 lacks the highly conserved arginine, indicating a novel interaction with phosphorylated PknD. Indeed, mutagenesis of other conserved residues within the domain was shown to have no effect on the observed phosphorylation (61), suggesting that Cpn0172, much like MxiG-N, does not have the canonical function of an FHA domain.

There is some evidence to suggest that the Chlamydias most closely represent the common ancestor of T3SSs (62–64), so it could be speculated that there has been a progressive loss of canonical FHA function during T3SS evolution if it is not

required for regulation. Indeed, the T3SS gene cluster of chlamydial species encodes a serine/threonine protein kinase, a prerequisite for signaling via Thr(P) recognition. In contrast, the only identified candidate for a serine/threonine protein kinase in *Shigella* spp. is the effector OspG, which is encoded on a distinct part of the virulence plasmid from *mxiG* and is likely to mediate its kinase activity within the host cell (65). However, the FHA fold is found in MxiG homologues across a wide spectrum of T3SSs, suggesting evolutionary conservation of a novel function. Indeed, our finding that overexpression of this domain fails to deregulate the T3SS suggests that the function of MxiG-N requires it to be localized within the T3SS and may not be regulatory at all. Thus, this domain appears to be an example of bacteria using a common structural scaffold for novel functionality. In addition, variation in domain function between T3SSs of different species may still exist, in the same way that regulation of secretion by threonine phosphorylation does not appear to be a ubiquitous feature of T6SSs (66).

All previously determined high resolution structures of basal body components are of periplasmic domains (17, 18, 20). Therefore, all docking into available EM maps has been focused on a region of density that corresponds to a hetero-oligomeric protein complex (16, 18, 19, 67). Additionally, because there are only high resolution structures for MxiM (13, 14) available for the *S. flexneri* basal body, docking into the EM map has had to rely on ring models from *Salmonella* and *Escherichia* (19), so any species-specific variation in the organization of the T3SS has not been considered. Therefore, previous estimates of the stoichiometry of basal body components based on docking into EM maps are understandably ambiguous. MxiG-N is the predominant basal body structure in the cytoplasm, so positioning of our solution structure has the potential to provide a relatively unambiguous estimate of the maximum number of copies of MxiG within the IMR. Indeed, the *S. flexneri* EM map shows clear density for leg domains at the base of the NC (supplemental Fig. 5*A*) (19), and there is good evidence that this region corresponds to the N-terminal domain of PrgH in *S. typhimurium* (16). Positioning of MxiG-N(6–112) within this density in the C24 *S. flexneri* NC EM map (19) shows a good agreement between the size of MxiG-N(6–112) and the density envelope. 24 copies are required to fully account for the volume of the MxiG-N ring, providing support for models that suggest a 24-fold symmetry for MxiG in the IMR (16, 17, 19). During preparation of this paper, a precise docking of the periplasmic domains of the basal body components into a 10 Å reconstruction of the *S. typhimurium* NC has been published (68). This also supports a model with 24 copies of MxiG homologues in the IMR of the T3SS. However, higher resolution EM maps are still required to precisely define the orientation of MxiG-N because this region is blurred out in the *Salmonella* reconstruction, presumably due to averaging of the different observed conformational states of MxiG-N (68).

Our 24-subunit ring models would suggest a close association of MxiG-N domains within the IMR, supported by surface and charge complementarity between opposing faces of the solution structure. This appears to contradict our finding that MxiG-N(6–112) is monomeric in a solution of up to 5 mM. However, MxiG is effectively localized at a high concentration within the physiological context of the IMR, so lower affinity interactions in the millimolar range could play a role in stabilization once the ring is assembled. Indeed, the effective molarity of MxiG-N(6–112) within the IMR can be estimated to be 80 mM, assuming a volume of ~500,000 $Å^3$ and a stoichiometry of 24 subunits for the MxiG-N ring. However, higher affinity binding events would probably be required for a contribution to initial assembly of the basal body.

The best resolution of features within the *S. flexneri* NC has been achieved by applying 12-fold symmetry during the EM reconstruction. This produced a map in which the outer portion of the IMR is seen to consist of 12 asymmetric dimers with pseudo-24-fold symmetry in the periplasmic region, leading to a model for the IMR where 12 copies of an asymmetric MxiG dimer are present (19). However, the density corresponding to the cytoplasmic (leg) portion only displays 12-fold symmetry (supplemental Fig. 5*B*). It is therefore unclear how to position 24 copies of MxiG-N(6–112) into the C12 map. Determination of whether this is a genuine feature of the *S. flexneri* T3SS or an artifact of the current C12 map will require higher resolution reconstructions.

In conclusion, our structure reveals MxiG-N to have an FHA fold, providing a starting point for investigating possible functions of this prominent yet largely uncharacterized T3SS domain in assembly and secretion. This work shows that *in vivo* phospho-recognition at the conserved FHA binding site is unlikely. Therefore, any involvement of MxiG-N in cell signaling must occur via a novel mechanism, suggesting that the bacterial T3SS has adopted the FHA fold for a non-canonical function. Elucidating the role of the FHA fold within MxiG homologues could provide key insights into the general function and evolution of this widespread building block in bacterial cell signaling. Our structure of the predominant cytoplasmic basal body component has facilitated an evaluation of proposed models for IMR arrangement. An estimate of stoichiometry based on the structure of MxiG-N(6–112) supports a model with 24 copies of MxiG, but higher resolution EM structures are still needed. Therefore, each new piece of data still has the potential to provide significant insight into the arrangement of this complex nanomachine.

Acknowledgment—We thank Devon Sheppard for helpful discussions about the NMR experiments.

REFERENCES

1. Cornelis, G. R. (2010) *Biol. Chem.* **391,** 745–751
2. Kotloff, K. L., Winickoff, J. P., Ivanoff, B., Clemens, J. D., Swerdlow, D. L., Sansonetti, P. J., Adak, G. K., and Levine, M. M. (1999) *Bull. World Health Organ.* **77,** 651–666
3. Morita-Ishihara, T. (2007) *Biosci. Microflora* **26,** 29–36
4. Kubori, T., Matsushima, Y., Nakamura, D., Uralil, J., Lara-Tejero, M., Sukhan, A., Galán, J. E., and Aizawa, S. I. (1998) *Science* **280,** 602–605
5. Blocker, A., Komoriya, K., and Aizawa, S. (2003) *Proc. Natl. Acad. Sci. U.S.A.* **100,** 3027–3030
6. Blocker, A. J., Deane, J. E., Veenendaal, A. K., Roversi, P., Hodgkinson, J. L., Johnson, S., and Lea, S. M. (2008) *Proc. Natl. Acad. Sci. U.S.A.* **105,** 6507–6513
7. Cordes, F. S., Komoriya, K., Larquet, E., Yang, S., Egelman, E. H., Blocker, A., and Lea, S. M. (2003) *J. Biol. Chem.* **278,** 17103–17107

8. Cordes, F. S., Daniell, S., Kenjale, R., Saurya, S., Picking, W. L., Picking, W. D., Booy, F., Lea, S. M., and Blocker, A. (2005) *J. Mol. Biol.* **354,** 206–211
9. Deane, J. E., Cordes, F. S., Roversi, P., Johnson, S., Kenjale, R., Picking, W. D., Picking, W. L., Lea, S. M., and Blocker, A. (2006) *Acta Crystallogr. Sect. F Struct. Biol. Cryst. Commun.* **62,** 302–305
10. Tamano, K., Aizawa, S., Katayama, E., Nonaka, T., Imajoh-Ohmi, S., Kuwae, A., Nagai, S., and Sasakawa, C. (2000) *EMBO J.* **19,** 3876–3887
11. Schuch, R., and Maurelli, A. T. (2001) *J. Bacteriol.* **183,** 6991–6998
12. Blocker, A., Jouihri, N., Larquet, E., Gounon, P., Ebel, F., Parsot, C., Sansonetti, P., and Allaoui, A. (2001) *Mol. Microbiol.* **39,** 652–663
13. Lario, P. I., Pfuetzner, R. A., Frey, E. A., Creagh, L., Haynes, C., Maurelli, A. T., and Strynadka, N. C. (2005) *EMBO J.* **24,** 1111–1121
14. Okon, M., Moraes, T. F., Lario, P. I., Creagh, A. L., Haynes, C. A., Strynadka, N. C., and McIntosh, L. P. (2008) *Structure* **16,** 1544–1554
15. Kimbrough, T. G., and Miller, S. I. (2000) *Proc. Natl. Acad. Sci. U.S.A.* **97,** 11008–11013
16. Schraidt, O., Lefebre, M. D., Brunner, M. J., Schmied, W. H., Schmidt, A., Radics, J., Mechtler, K., Galán, J. E., and Marlovits, T. C. (2010) *PLoS Pathog* **6,** e1000824
17. Yip, C. K., Kimbrough, T. G., Felise, H. B., Vuckovic, M., Thomas, N. A., Pfuetzner, R. A., Frey, E. A., Finlay, B. B., Miller, S. I., and Strynadka, N. C. (2005) *Nature* **435,** 702–707
18. Spreter, T., Yip, C. K., Sanowar, S., André, I., Kimbrough, T. G., Vuckovic, M., Pfuetzner, R. A., Deng, W., Yu, A. C., Finlay, B. B., Baker, D., Miller, S. I., and Strynadka, N. C. (2009) *Nat. Struct. Mol. Biol.* **16,** 468–476
19. Hodgkinson, J. L., Horsley, A., Stabat, D., Simon, M., Johnson, S., da Fonseca, P. C., Morris, E. P., Wall, J. S., Lea, S. M., and Blocker, A. J. (2009) *Nat. Struct. Mol. Biol.* **16,** 477–485
20. Crepin, V. F., Prasannan, S., Shaw, R. K., Wilson, R. K., Creasey, E., Abe, C. M., Knutton, S., Frankel, G., and Matthews, S. (2005) *Mol. Microbiol.* **55,** 1658–1670
21. Allaoui, A., Sansonetti, P. J., Ménard, R., Barzu, S., Mounier, J., Phalipon, A., and Parsot, C. (1995) *Mol. Microbiol.* **17,** 461–470
22. Sani, M., Allaoui, A., Fusetti, F., Oostergetel, G. T., Keegstra, W., and Boekema, E. J. (2007) *Micron* **38,** 291–301
23. Marlovits, T. C., Kubori, T., Sukhan, A., Thomas, D. R., Galán, J. E., and Unger, V. M. (2004) *Science* **306,** 1040–1042
24. Allaoui, A., Sansonetti, P. J., and Parsot, C. (1992) *J. Bacteriol.* **174,** 7661–7669
25. Plano, G. V., and Straley, S. C. (1995) *J. Bacteriol.* **177,** 3843–3854
26. Ross, J. A., and Plano, G. V. (2011) *J. Bacteriol.* **193,** 2276–2289
27. Bax, A., and Ikura, M. (1991) *J. Biomol. NMR* **1,** 99–104
28. Grzesiek, S., and Bax, A. (1992) *J. Am. Chem. Soc.* **114,** 6291–6293
29. Grzesiek, S., and Bax, A. (1992) *J. Magn. Reson. (1969)* **99,** 201–207
30. Kay, L. E., Ikura, M., Tschudin, R., and Bax, A. (1990) *J. Magn. Reson. (1969)* **89,** 496–514
31. Farmer, B. T., and Venters, R. A. (1995) *J. Am. Chem. Soc.* **117,** 4187–4188
32. Goddard, T. D., and Kneller, D. G. SPARKY 3, University of California, San Francisco
33. Marion, D., Driscoll, P. C., Kay, L. E., Wingfield, P. T., Bax, A., Gronenborn, A. M., and Clore, G. M. (1989) *Biochemistry* **28,** 6150–6156
34. Wüthrich, K., Billeter, M., and Braun, W. (1984) *J. Mol. Biol.* **180,** 715–740
35. Cordier, F., Nisius, L., Dingley, A. J., and Grzesiek, S. (2008) *Nat. Protoc.* **3,** 235–241
36. Shen, Y., Delaglio, F., Cornilescu, G., and Bax, A. (2009) *J. Biomol. NMR* **44,** 213–223
37. Güntert, P., Mumenthaler, C., and Wüthrich, K. (1997) *J. Mol. Biol.* **273,** 283–298
38. Meitert, T., Pencu, E., Ciudin, L., Tonciu, M., Mihai, I., and Nicolescu, S. (1991) *Roum. Arch. Microbiol. Immunol.* **50,** 45–52
39. Kenjale, R., Wilson, J., Zenk, S. F., Saurya, S., Picking, W. L., Picking, W. D., and Blocker, A. (2005) *J. Biol. Chem.* **280,** 42929–42937
40. Zenk, S. F., Stabat, D., Hodgkinson, J. L., Veenendaal, A. K., Johnson, S., and Blocker, A. J. (2007) *Microbiology* **153,** 2405–2415
41. Emsley, P., Lohkamp, B., Scott, W. G., and Cowtan, K. (2010) *Acta Crystallogr. D* **66,** 486–501
42. Kleywegt, G. J., and Jones, T. A. (1996) *Acta Crystallogr. D* **52,** 826–828
43. CCP4 (1994) *Acta Crystallogr. D* **50,** 760–763
44. Altschul, S. F., Gish, W., Miller, W., Myers, E. W., and Lipman, D. J. (1990) *J. Mol. Biol.* **215,** 403–410
45. Canutescu, A. A., Shelenkov, A. A., and Dunbrack, R. L., Jr. (2003) *Protein Sci.* **12,** 2001–2014
46. Baker, N. A., Sept, D., Joseph, S., Holst, M. J., and McCammon, J. A. (2001) *Proc. Natl. Acad. Sci. U.S.A.* **98,** 10037–10041
47. Holm, L., and Sander, C. (1993) *J. Mol. Biol.* **233,** 123–138
48. Tsai, M. D. (2002) *Structure* **10,** 887–888
49. Pallen, M., Chaudhuri, R., and Khan, A. (2002) *Trends Microbiol.* **10,** 556–563
50. Hammet, A., Pike, B. L., McNees, C. J., Conlan, L. A., Tenis, N., and Heierhorst, J. (2003) *IUBMB Life* **55,** 23–27
51. Lee, H., Yuan, C., Hammet, A., Mahajan, A., Chen, E. S., Wu, M. R., Su, M. I., Heierhorst, J., and Tsai, M. D. (2008) *Mol. Cell* **30,** 767–778
52. Alderwick, L. J., Molle, V., Kremer, L., Cozzone, A. J., Dafforn, T. R., Besra, G. S., and Fütterer, K. (2006) *Proc. Natl. Acad. Sci. U.S.A.* **103,** 2558–2563
53. Byeon, I. J., Li, H., Song, H., Gronenborn, A. M., and Tsai, M. D. (2005) *Nat. Struct. Mol. Biol.* **12,** 987–993
54. Durocher, D., Taylor, I. A., Sarbassova, D., Haire, L. F., Westcott, S. L., Jackson, S. P., Smerdon, S. J., and Yaffe, M. B. (2000) *Mol. Cell* **6,** 1169–1182
55. Molle, V., Kremer, L., Girard-Blanc, C., Besra, G. S., Cozzone, A. J., and Prost, J. F. (2003) *Biochemistry* **42,** 15300–15309
56. Parsot, C., Ménard, R., Gounon, P., and Sansonetti, P. J. (1995) *Mol. Microbiol.* **16,** 291–300
57. Bahrani, F. K., Sansonetti, P. J., and Parsot, C. (1997) *Infect. Immun.* **65,** 4005–4010
58. Mahajan, A., Yuan, C., Lee, H., Chen, E. S., Wu, P. Y., and Tsai, M. D. (2008) *Sci. Signal.* **1,** re12
59. Betts, H. J., Twiggs, L. E., Sal, M. S., Wyrick, P. B., and Fields, K. A. (2008) *J. Bacteriol.* **190,** 1680–1690
60. Mougous, J. D., Gifford, C. A., Ramsdell, T. L., and Mekalanos, J. J. (2007) *Nat. Cell Biol.* **9,** 797–803
61. Johnson, D. L., and Mahony, J. B. (2007) *J. Bacteriol.* **189,** 7549–7555
62. Kim, J. F. (2001) *Trends Genet.* **17,** 65–69
63. Gophna, U., Ron, E. Z., and Graur, D. (2003) *Gene* **312,** 151–163
64. Pallen, M. J., Beatson, S. A., and Bailey, C. M. (2005) *FEMS Microbiol. Rev.* **29,** 201–229
65. Kim, D. W., Lenzen, G., Page, A. L., Legrain, P., Sansonetti, P. J., and Parsot, C. (2005) *Proc. Natl. Acad. Sci. U.S.A.* **102,** 14046–14051
66. Bingle, L. E., Bailey, C. M., and Pallen, M. J. (2008) *Curr. Opin. Microbiol.* **11,** 3–8
67. Sanowar, S., Singh, P., Pfuetzner, R. A., André, I., Zheng, H., Spreter, T., Strynadka, N. C., Gonen, T., Baker, D., Goodlett, D. R., and Miller, S. I. (2010) *m.Bio.* **1,** e00158–10
68. Schraidt, O., and Marlovits, T. C. (2011) *Science* **331,** 1192–1195
69. Davis, I. W., Leaver-Fay, A., Chen, V. B., Block, J. N., Kapral, G. J., Wang, X., Murray, L. W., Arendall, W. B., 3rd, Snoeyink, J., Richardson, J. S., and Richardson, D. C. (2007) *Nucleic Acids Res.* **35,** W375–W383
70. Sansonetti, P. J., Kopecko, D. J., and Formal, S. B. (1982) *Infect. Immun.* **35,** 852–860